Q. J. R. Meteorol. Soc. (2000), 126, pp. 1239–1260

Biosphere–atmosphere interactions over West Africa. I: Development and validation of a coupled dynamic model

By GUILING WANG* and ELFATIH A. B. ELTAHIR
Massachusetts Institute of Technology, USA

(Received 12 April 1999; revised 7 September 1999)

SUMMARY

In this study we develop a zonally symmetric, synchronously coupled biosphere–atmosphere model including ecosystem dynamics, and apply this model to study biosphere–atmosphere interactions in the region of West Africa. The atmospheric model is zonally symmetric, and includes representation of atmospheric dynamics, a radiation scheme, a moist convection scheme, a boundary-layer scheme, and a cloud-parametrization scheme. The biospheric model is the Integrated BIosphere Simulator (IBIS), which includes representation of the water, energy, momentum, and carbon balance, vegetation phenology, and vegetation dynamics. We modified the representation of canopy hydrology in IBIS to account for the impact of rainfall subgrid variability. The biospheric model and atmospheric model are separately tested against observations. The synchronously coupled model is then used to simulate the biosphere–atmosphere system of West Africa. A study on the role of biosphere–atmosphere interactions, including ecosystem dynamics, in the climate variability over West Africa using this model will be presented in a companion paper.

KEYWORDS: Biosphere–atmosphere interactions Drought Ecosystem dynamics West Africa

1. INTRODUCTION

In the past two decades, significant scientific effort has been devoted to the study of the severe persistent drought in West Africa which started in the late 1960s. Among other factors, land-surface feedback triggered by man-made desertification is widely viewed as a possible mechanism for the drought occurrence and its persistence. Studies on land-surface feedback were pioneered by Charney (1975). He proposed a biogeophysical feedback hypothesis: the cooling effect due to albedo increase caused by desertification enhances local subsidence, thus reducing the precipitation, which further limits the vegetation growth and makes the drought self-sustaining. This hypothesis was followed by numerous modelling studies on the climatic impact of land-cover changes such as desertification in the Sahel (e.g. Charney *et al.* 1977; Sud and Molod 1988; Xue and Shukla 1993; Zheng and Eltahir 1997, 1998) and deforestation in the Amazon Basin (e.g. Dickinson and Henderson-Sellers 1988; Shukla *et al.* 1990; Henderson-Sellers *et al.* 1993; Zeng *et al.* 1996; Zhang and Henderson-Sellers 1996) and tropical Africa (e.g. Zhang and Henderson-Sellers 1996; Zheng and Eltahir 1997, 1998). A common conclusion has been drawn that vegetation degradation reduces precipitation and moisture convergence. It has also been concluded that the climate system in West Africa is sensitive to changes of land cover.

Previous studies on the climatic impact of land-cover changes have made important contributions to understanding the role that vegetation plays in the climate system. However, in the models used by these studies, the vegetation state was prescribed; therefore, the response of vegetation to the induced climate change was not included. Correspondingly, conclusions based on these studies are subject to the condition of assuming permanent land-cover changes. In reality, depending upon the nature of the vegetation perturbation, the post-disturbance landscape may have a certain degree of freedom to respond in a natural way. For example, forest harvesting usually takes place with a rotation cycle of several decades; farms are reclaimed by grasses or trees upon agricultural abandonment; livestock tends to migrate when a region is overgrazed; dense

* Corresponding author: Ralph M. Parsons Laboratory, 48-208, Massachusetts Institute of Technology, Cambridge, MA 02139, USA. e-mail: glwang@mit.edu

ground vegetation colonizes the land surface even in the first year following a sweeping fire; and so on. In these cases there exists an active two-way biosphere–atmosphere feedback involving vegetation dynamics, without which the cycle associated with the biogeophysical feedback in Charney's hypothesis cannot be closed.

The importance of vegetation dynamics is not limited to the scenario of anthropogenic perturbations. The drought in the twentieth century is not the first in West Africa. The Sahel region experienced several similar droughts during the past three to four centuries (Nicholson 1981), long before human activity started significantly to impact the ecological balance over that region. The vegetation degradation caused by these drought events is expected to impose a long-term effect on the regional climate through biosphere–atmosphere interactions. Understanding the relevant processes involved in this natural biosphere–atmosphere system is the key to understanding the long-term climate variability as well as the current climate. Vegetation dynamics are among the most important of these processes. The role of vegetation dynamics has also been highlighted in studies on the paleoclimatology of West Africa (Kutzbach *et al.* 1996a,b; Texier *et al.* 1997; Brostrom *et al.* 1998). For example, Kutzbach *et al.* (1996a) simulated the African monsoon in the middle Holocene, and their results suggested that climate models need to include the biospheric processes involving the climate-related changes in both the vegetation and the soil.

The vegetation response to climate forcings has been incorporated into climate models by a few recent studies (Claussen 1994, 1997; Lofgren 1995a,b), which used equilibrium biome models to predict the vegetation and land-surface parameters. However, equilibrium biome models can only predict the equilibrium vegetation, and do not simulate vegetation dynamics. It is not until the emergence of fully dynamic biospheric models such as the Integrated BIosphere Simulation (IBIS) (Foley *et al.* 1996) that development of a synchronously coupled biosphere–atmosphere model including vegetation dynamics became possible. Recently, Foley *et al.* (1998) coupled the GENESIS-AGCM* model with IBIS and reproduced the current climate reasonably well, which signalled the success of incorporating vegetation dynamics into climate models. Here and in what follows, we use the term 'climate' to stand for the long-term mean of environmental conditions, not only in the atmosphere but also in the biosphere.

The recent advances in modelling the synchronous coupling between the biosphere and the atmosphere make it possible to pursue studies on the impact of land-cover changes within the scope of a natural, dynamic ecosystem. We are interested in how the biosphere and the atmosphere as a synchronously coupled system respond to non-permanent vegetation perturbations over West Africa. Owing to the slow nature of vegetation growth and decay, the time-scale associated with ecosystem dynamics can easily be decades long. To better serve our research purpose, we developed a zonally symmetric model of the synchronously coupled biosphere–atmosphere system, which is computationally more efficient than a 3-D model of the same kind. As documented by Zheng and Eltahir (1998), the observed climatic conditions justify the assumption of zonal symmetry in West Africa.

In this paper, we concentrate on the development and validation of a Zonally symmetric, synchronously coupled Biosphere–Atmosphere Model (ZonalBAM). Each component of the model is described first. The biospheric model and the atmospheric model are then separately tested against observations: driven by the climatological atmospheric forcings, the biosphere model is run in a stand-alone mode to reproduce the potential vegetation in West Africa; with vegetation fixed at its current condition,

* Atmospheric General Circulation Model.

the biosphere–atmosphere model is run to reproduce the current atmospheric climate over West Africa. Finally, the full model is used to simulate the biosphere–atmosphere system including ecosystem dynamics. Further studies using this model are presented in a companion paper (Wang and Eltahir 2000).

2. MODEL DEVELOPMENT

The newly developed model ZonalBAM describes the coupled biosphere–atmosphere system over West Africa including ecosystem dynamics. It includes a zonally symmetric atmospheric model and a fully dynamic biospheric model, which will be described in the following.

(a) *The atmospheric model*

The development of the atmospheric model started from the framework of the zonally symmetric atmospheric model of Zheng (1997), which has been used in several previous studies (Zheng and Eltahir 1997, 1998; Zheng 1998; Zheng *et al.* 1999). The atmospheric dynamics in the Zheng (1997) model follows Plumb and Hou (1992). It uses $z = -H \ln(p/p_s)$ (i.e. log-pressure) as the vertical coordinate and $y = a \sin \phi$ as the meridional coordinate. Here H is a reference scale-height (we use 8 km), p the pressure, p_s the reference pressure (usually taken as 1000 mb), a the earth radius, and ϕ the latitude. In the vertical direction, the Zheng (1997) model assumed uniform resolution with respect to height. We modified the numerical scheme for the atmospheric dynamics so that the model can have a non-uniform vertical resolution, which adds to the computational efficiency of the model. In the meridional direction, the model domain covers the whole globe, with the resolution determined by uniformly dividing the $a \sin \phi$ axis. The land–ocean boundary is set at 6°N, with land in the north and ocean in the south. Sea surface temperature is prescribed according to the observations.

For atmospheric physics, similar to Zheng (1997), we use the radiation scheme by Chou *et al.* (1991) and Chou (1992), and the convection scheme by Emanuel (1991) (version 4.1), which are briefly described in the following. Here our model development focuses on the representation of additional physical processes, including the cloud–radiation feedback and atmospheric boundary-layer processes.

(i) *Radiation scheme and convection scheme*

The radiation parametrization scheme computes the infrared and solar-radiation fluxes at different absorption bands (or spectral regions), and derives the overall solar-heating and thermal-cooling rate in the atmosphere. For the infrared radiation, this scheme considers the absorption and emission in different H_2O bands, the CO_2 band and the O_3 band, as well as the effect of CH_4 and N_2O. For the solar radiation, it accounts for the absorption by H_2O, CO_2, and O_3. For both the solar and infrared radiation, the impact of clouds is included. Details about the infrared radiation calculation can be found in Chou (1984), Chou *et al.* (1991) and Chou and Kouvaris (1991); details about the solar radiation can be found in Chou (1986, 1990, 1992).

The moist convection processes are simulated using the convection scheme developed by Emanuel (1991). We are using the recently updated version CONVECT 4.1. In this scheme, the convection representation is mainly based on the dynamics and microphysics of the cloud processes, which are deduced from recent observations and theories of convective clouds. The fundamental entities of convective transport are the subcloud-scale draughts rather than the clouds themselves. The main closure parameters are the parcel precipitation efficiencies, φ and ψ: φ determines how much of the condensed water is converted to precipitation; ψ determines how much of the precipitation falls through the unsaturated air thus leading to warming and drying, while the remaining fraction $(1 - \psi)$ of the precipitation re-evaporates, leading to cooling and moistening. These parameters are specified as functions of altitude, temperature, and adiabatic water content, thus relating the large-scale forcings to the microphysics of cloud processes. Given the vertical profile of temperature and humidity, the convection scheme computes the amount of convective precipitation and the tendencies of temperature and moisture. Further details can be found in Emanuel (1991). Large-scale condensation is treated separately from convection. When the atmosphere reaches supersaturation, the excess water is condensed out of the system as large-scale precipitation, and no re-evaporation is considered. During both the convection and large-scale condensation processes, enthalpy is conserved.

(ii) *Cloud parametrization scheme*

This study takes a highly simplified approach towards the representation of cloud–radiation feedback. Clouds in this model are divided into three groups: high-level clouds, medium-level clouds, and low-level clouds. According to London (1952), the globally averaged vertical expansion for the high-, medium- and low-level clouds are 220–280 mb, 460–640 mb and 640–940 mb, and the optical depths of each cloud type are about 2, 6 and 12, respectively. We fix both the cloud vertical expansions and the cloud optical depths at their global means. Only the fractional cloud cover is predicted by the model.

The parametrization of the fractional cloud cover is developed based on Kvamsto (1991). Previous studies (e.g. Slingo 1980, 1987; Sunquist 1989; Kvamsto 1991) have developed many fractional-cloudiness parametrization schemes. Some of these are complex and consider the impact of several physical variables, while others predict the cloudiness based on one single variable, the relative humidity. The Kvamsto (1991) scheme belongs to the latter group. It features a linear relationship between the relative humidity and the fractional coverage of the low-level clouds, as described by the following:

$$\mathrm{FC} = \max\left(0.0, \frac{\mathrm{RH} - \mathrm{RH_0}}{1 - \mathrm{RH_0}}\right), \tag{1}$$

where FC is the cloud fractional cover, RH is the relative humidity, and $\mathrm{RH_0}$ is the relative-humidity threshold at which clouds start to form. Despite its simplicity, the performance of the Kvamsto scheme is one of the best among the seven schemes examined by Mocko and Cotton (1995). Here we adapt the linear scheme shown in Eq. (1) for the low-level clouds and expand its application to the medium- and high-level clouds. For the relative humidity threshold $\mathrm{RH_0}$, we use 0.8, 0.65 and 0.7 for high-, medium- and low-level clouds, respectively. Because of the difference in spatial resolution, these threshold values are slightly lower than those usually used in mesoscale models.

(iii) *Boundary-layer scheme*

Boundary-layer processes play an important role in biosphere–atmosphere interactions. The free atmosphere 'feels' the existence of the surface through the growth and decay of the boundary layer which responds to surface forcings through turbulence. Heating from the warm ground and wind shear near the surface due to frictional drag all contribute to the generation of turbulence. Within the boundary layer, the transport of quantities such as heat, moisture, and momentum in the vertical direction is dominated by turbulent transport, which is orders of magnitude more efficient than the transport through molecular diffusion. The objective of boundary-layer models is to describe these turbulent transports.

We use the 'non-local' boundary-layer scheme based on Holtslag and Boville (1993). The Hotslag and Boville (1993) scheme is labelled 'non-local' mainly because the formulation of the eddy diffusivity depends on the bulk properties of the atmospheric boundary layer, instead of the local properties. It can also incorporate the 'non-local' vertical transport for heat and moisture due to convection. As shown by Holtslag and Boville (1993) in a global climate model, the performance of a 'non-local' scheme is in general better than that of a 'local' boundary-layer scheme.

The turbulent transport of heat, moisture and momentum can be expressed by the following equations:

$$\frac{\mathrm{d}\theta}{\mathrm{d}t} = \frac{\partial}{\partial z} K_h \left(\frac{\partial \theta}{\partial z} - G_h \right), \tag{2}$$

$$\frac{\mathrm{d}q}{\mathrm{d}t} = \frac{\partial}{\partial z} K_q \left(\frac{\partial q}{\partial z} - G_q \right), \tag{3}$$

$$\frac{\mathrm{d}u}{\mathrm{d}t} = \frac{\partial}{\partial z} K_m \left(\frac{\partial u}{\partial z} \right), \tag{4}$$

$$\frac{\mathrm{d}v}{\mathrm{d}t} = \frac{\partial}{\partial z} K_m \left(\frac{\partial v}{\partial z} \right), \tag{5}$$

where θ is temperature, q is water content, and u and v are horizontal velocities; K_h, K_q and K_m are the eddy diffusivities for heat, water vapour and momentum, respectively, and G_h and G_q represent the non-local transport for heat and water vapour, respectively. The eddy diffusivity depends on the level z and the boundary layer height h, formulated as:

$$K_{h,q,m} = k\omega z \left(1 - \frac{z}{h}\right)^2,$$

where k is the von Karman constant, and ω is a characteristic turbulent velocity-scale. The boundary-layer height h is determined by an implicit relationship between h and the bulk Richardson number:

$$h = \frac{Ri_{\mathrm{cr}}(u(h)^2 + v(h)^2)}{(g/\theta_{\mathrm{s}})(\theta_{\mathrm{v}}(h) - \theta_{\mathrm{s}})},$$

where θ_{s} is the air temperature near the surface, θ_{v} is the virtual temperature, and Ri_{cr} is the critical Richardson number, usually between 0.25 and 0.50.

(*b*) *The biospheric model*

The dynamic biospheric model uses IBIS, developed by Foley *et al.* (1996). IBIS integrates a wide range of terrestrial phenomena, including the biophysical, physiological, and ecosystem dynamical processes, into a single, physically consistent simulator that can be directly coupled to atmospheric models. IBIS takes the atmospheric forcings provided by the atmospheric model as inputs, returns information on surface properties and surface fluxes to the atmospheric model, while updating the biospheric state including the vegetation structure. Here we give a brief description of IBIS, followed by a description of the modification we have made on its representation of canopy hydrology.

(i) *IBIS description.* The vegetation cover in IBIS is a combination of different plant functional types (PFTs). PFTs are defined based on physiognomy (trees and grasses), leaf form (broad-leaf and needle-leaf), leaf habit (evergreen and deciduous), and photosynthetic pathway (C3 and C4). For example, PFTs that grow well in the Tropics include tropical broadleaf evergreen trees, tropical broadleaf drought-deciduous trees, and C4 grasses. Vegetation canopy is divided into two layers, with woody plants in the upper canopy and herbaceous plants in the lower canopy. Soil texture is represented by the percentage of three different components: sand, silt, and clay. There are six soil layers in the root zone, which sum up to 4.00 m. The thickness of each soil layer, from the top to the bottom, is 0.10, 0.15, 0.25, 0.50, 1.00, and 2.00 m respectively. The rooting profiles differ between different PFTs, and are based on published data (Jackson *et al.* 1996).

IBIS consists of four component modules: the land-surface module, the vegetation phenology module, the carbon-balance module, and the vegetation-dynamics module, as described in the following.

The land-surface module represents the biophysical and physiological processes at a time-step similar to that of the atmospheric model (20 minutes in our study). It solves for the exchange of water vapour, energy, carbon dioxide and momentum between the ground and vegetation, between different vegetation layers, and between vegetation and the atmosphere. Solar radiation is treated using two-stream approximations within each canopy layer; for infrared radiation, each canopy layer is treated as a semi-transparent plane with its emissivity dependent on the leaf and stem density. For the canopy hydrological processes, IBIS has a detailed description for the cascade of precipitation. Formulations for interception, throughfall, evaporation from the intercepted water, and plant transpiration are physically based. The overall evapotranspiration has three different components: evaporation from the ground surface, evaporation from the intercepted water, and transpiration from the vegetation canopy. The exchange of water vapour and carbon dioxide between vegetation canopies and the atmosphere is strongly related to photosynthesis and stomatal conductance. IBIS uses physiologically based formulations of C3 and C4 photosynthesis, stomatal conductance, and respiration.

Also described in this module are the exchange of water and energy between different soil layers. Relevant processes include heat diffusion, water transport, plant uptake for water, and so on. Water transport between different soil layers is governed by gravity drainage and diffusion. Direct evaporation from the soil only occurs in the top layer. The drainage from the bottom soil layer is modelled assuming gravity drainage and neglecting interactions with groundwater aquifers. Water uptake by plants from different soil layers depends on the rooting profiles. Water stress is considered when the soil moisture is below the wilting point.

The vegetation phenology module, operating at a daily time-step, describes the plant leaf display in relation to seasonal climate conditions. For example, winter-deciduous plants are assumed to shed their leaves when temperature drops below a threshold value; leaf-shedding for drought-deciduous plants takes place upon severe water stress.

The carbon-balance module calculates the net primary productivity (NPP) for each PFT, and updates their carbon storages at an annual time-step. The annual NPP is equal to the difference between photosynthesis and respiration, integrated through an entire year. NPP is allocated to three different carbon reservoirs: leaves, stems, and roots. The change of carbon biomass in each reservoir depends on the NPP allocation and the turnover rate. Parameters on allocation and turnover differ between different PFTs.

The vegetation-dynamics module updates the vegetation structure for each PFT at an annual time-step according to its carbon budget. Whether a PFT can potentially exist at a specific grid point depends on the climatic constraints; whether it can actually survive depends on its competition with other PFTs for common resources. The transient change in vegetation structure, including the leaf area index (LAI) and living biomass, is a reflection of this competition. Common resources account for water and light. The effect of nutrient stress is not considered.

PFTs in different canopy layers have different advantages in accessing light and water. The upper layer has easier access to sunlight, and shades the lower layer to a certain degree depending on its fractional coverage. Plants in the upper layer have deeper root structures than those in the lower layer. As a result, the lower-layer PFTs have the advantage of reaching water first in the process of infiltration, while the upper-layer PFTs have access to the water storage in the deeper soil.

Competition between PFTs within the same canopy layer has to do with the difference in their ecological strategies. For example, under severe water stress, drought-deciduous plants shed their leaves to shut off the water consumption through transpiration. Needle-leaf plants conserve water better than broadleaf plants. C4 plants use water more efficiently than C3 plants. These factors cause the carbon-balance difference between different PFTs in the same layer. More details about IBIS can be found in Foley *et al.* (1996).

(ii) *Subgrid heterogeneity*

Although IBIS has detailed and sophisticated representation for canopy hydrological processes, it does not consider the effect of subgrid variability in rainfall distribution. The spatial scale of a typical rain cell is $O(10^0)$ km, while the typical resolution for regional and global climate models is $O(10^2)$ to $O(10^3)$ km. Model rainfall is actually the average rainfall over the entire grid cell. As a result, the rainfall intensity in climate models is often much lower than observed. This bias, without proper treatment, will cause false representation of canopy hydrology, which has severe consequences in modelling both the biosphere and the atmosphere (Wang and Eltahir 1998). Therefore, we modified the representation of canopy hydrological processes in IBIS by including an interception scheme which accounts for the impact of rainfall subgrid variability.

Our interception scheme is based on the Shuttleworth scheme (1988b). Precipitation, P, is assumed to fall over a fraction μ of the grid cell. Within the rain-covered region, the probability density function for rainfall distribution takes the form:

$$f(P) = \frac{\mu}{P_0} \exp\left(-\frac{\mu P}{P_0}\right), \tag{6}$$

where P_0 is the grid-averaged precipitation rate. As a result, the grid-average rate of canopy infiltration can be derived as (refer to Shuttleworth (1988b) for details):

$$I = P_0 \left\{1 - \exp\left(-\frac{\mu I_{\max}}{P_0}\right)\right\}, \tag{7}$$

where $I_{\max} = (S - C)/\Delta t$, with S being the canopy capacity, C the canopy storage, and Δt the model time-step. Canopy runoff is then computed by summing up the instant throughfall (i.e. $P_0 - I$) and the slow dripping from the canopy storage.

According to previous studies (Pitman *et al.* 1990; Johnson *et al.* 1991; Thomas and Henderson-Sellers 1991), a model's climate is very sensitive to the choice of the parameter μ. Here, we use the Eltahir and Bras (1993) method to estimate the fractional

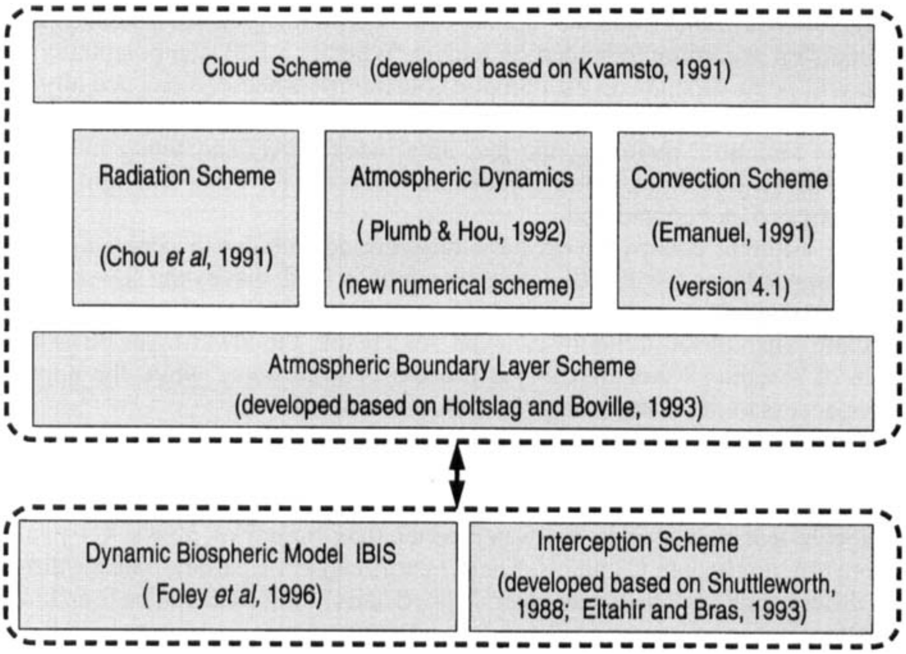

Figure 1. Components of the coupled biosphere–atmosphere model.

rainfall coverage:

$$\mu = \frac{P_{\mathrm{model}}}{P_{\mathrm{obs}}}, \tag{8}$$

where P_{model} is the modelled rainfall intensity, and P_{obs} is the climatology of observed rainfall intensity at the corresponding location and during the corresponding season. We estimate P_{obs} based on published data in Lebel *et al.* (1997) and Le Barbe and Lebel (1997). This method of estimating μ guarantees that the simulated climatology of precipitation intensity over the rain-covered region is always close to observations, and allows μ to vary with time and location, bringing greater physical realism into the model.

To summarize the model development, Fig. 1 shows all the components of the coupled biosphere–atmosphere model ZonalBAM.

3. Model validation

Two experiments are carried out to separately test the biospheric model and the atmospheric model against observations: the biospheric model is run in an off-line mode to simulate the potential vegetation in West Africa; the coupled biosphere–atmosphere model is run with vegetation fixed at today's condition to simulate the atmospheric climate.

(*a*) *Modelling the biosphere*

By driving IBIS with the climatological atmospheric forcings, Foley *et al.* (1996) used the stand-alone IBIS to reproduce the global vegetation distribution. Here we perform a similar study, but with the newly modified representation of canopy hydrology

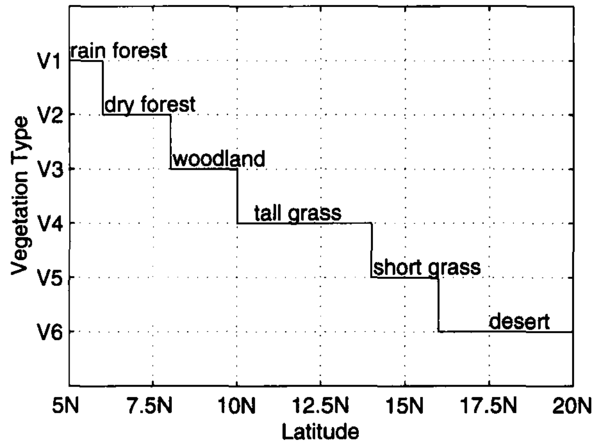

Figure 2. Vegetation type after the biosphere reaches equilibrium. V1 represents forest dominated by tropical broadleaf evergreen trees; V2 represents forest dominated by tropical broadleaf drought-deciduous trees; V3 represents woody plants dominated by tropical broadleaf drought-deciduous trees but less dense than forest; V4 stands for dense tall C4 grass; V5 stands for short C4 grass; V6 stands for desert condition.

and with different atmospheric forcings. For the atmospheric forcings, we use the daily climatology from the NCEP/NCAR* reanalysis data (Kalnay *et al.* 1996). The daily climatology is derived based on the data for 1958–1997, and averaged between 15°W and 15°E. The temperature and specific humidity are interpolated into finer temporal resolution by assuming a sinusoidal diurnal cycle. Following Foley *et al.* (1996), the daily precipitation is assumed to occur within a certain time period, and the length of precipitation event as well as the starting time is randomly determined. Different from the simulations involving the atmospheric model, the incoming solar radiation and the incoming long-wave radiation in the off-line IBIS are calculated based on their empirical relationships with the fractional cloud cover.

With the spatial resolution of 2°, the model domain spans from 5°N to 25°N. The time-step for the land surface processes is 30 minutes. Simulation starts with minimal vegetation cover everywhere. At the beginning, each of the PFTs has an equal opportunity to survive—all of them exist at every grid point, with the same LAI of 0.1 in order for the physiological processes to get started. The stem and root biomass are initialized to be zero. Later on, the vegetation distribution depends on the competition between PFTs for light and water under the corresponding atmospheric conditions. Here the soil texture is fixed with time, and varies from silty loam (20% sand, 60% silt, 20% clay) near the coast to loamy sand (80% sand, 10% silt, 10% clay) in the north, according to the Zobler (1986) data.

After 80 years of simulation, the model evolves very close to equilibrium. The competition between grasses and trees comes to an end, and the net primary productivity remains stable. The only process that has not reached an equilibrium state is the slow accumulation of woody biomass, which has a time-scale in the order of centuries. Details of this equilibrium vegetation distribution are presented in Fig. 2. At equilibrium, trees exist between the coast and 10°N, while grasses occupy the region between 10°N and 16°N. North of that, the land surface features desert condition. Figure 3 shows the simulated NPP, with the mean and standard deviation of point measurements (Murphy 1975) from humid and arid regions in West Africa. The statistics for each region are

* National Centers for Environmental Prediction/National Center for Atmospheric Research.

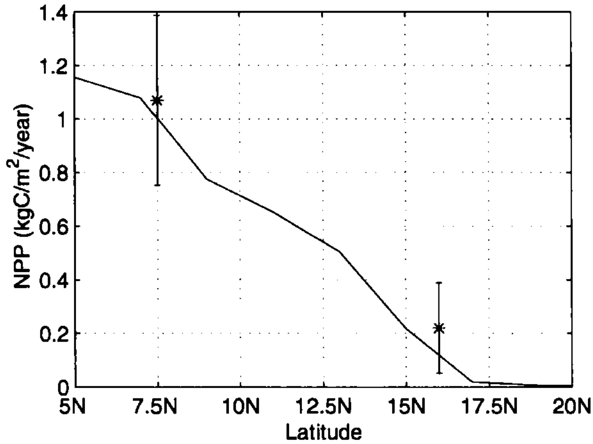

Figure 3. The total net primary productivity at the biosphere equilibrium. The two asterisks with error bars mark the mean and standard deviation of point measurements (Murphy 1975) from humid and arid regions in West Africa.

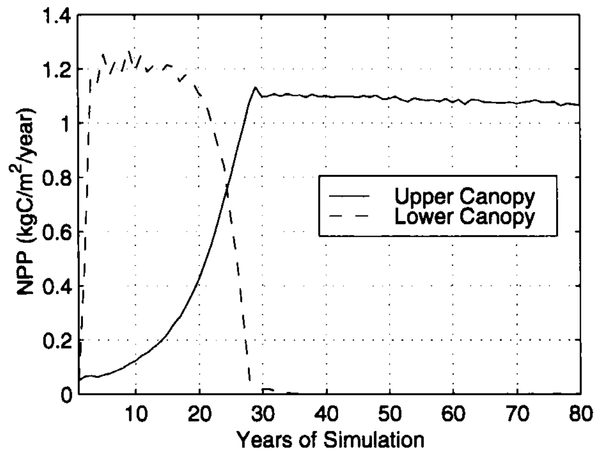

Figure 4. The net primary productivity of the upper and lower canopy at 7°N. This reflects the competition between the woody plants and herbaceous plants.

based on five site measurements. Our simulation is in fair agreement with the site measurements.

Over locations that are eventually occupied by trees, competition between trees and grasses took place before the establishment of trees. As an example, Fig. 4 presents the NPP by the upper canopy and the NPP by the lower canopy at 7°N. The early stage of vegetation development is dominated by highly productive grasses. Trees gradually take over and grasses die out within three decades. After that the tree NPP stays stable.

In general, the simulated vegetation captures the main features of the landscape in West Africa. As Foley *et al.* (1996) already found, due to the lack of disturbance mechanism and climate variability, the model does not do well in simulating the savannah-type vegetation (i.e. a mixture between trees and grasses). As shown in Fig. 2, tall grasses exist right next to the dense woodland.

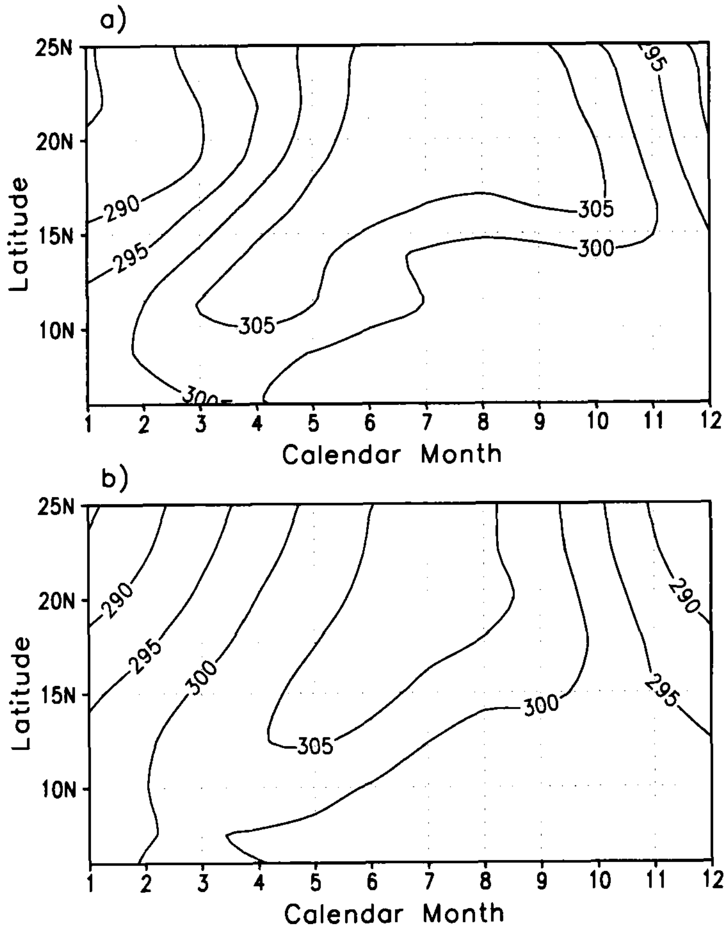

Figure 5. The seasonal cycle of surface temperature (K): (a) the model simulation; (b) climatology of the NCEP re-analysis data.

(*b*) *Modelling the atmosphere*

With the ecosystem dynamics being turned off and vegetation fixed at close to today's condition, the biosphere–atmosphere model is used to simulate the current atmospheric climate over West Africa. Under this condition, the biospheric model IBIS functions as a sophisticated land-surface model with static vegetation. Here the static vegetation only means that vegetation does not change from one year to the next. The diurnal cycle and seasonal cycle are still simulated for the biophysical, physiological, and phenological processes.

Over West Africa, there is evergreen rain forest immediately off the coast. Drought-deciduous forest and woodland extend from the coast to about 10°N, from where the vegetation gradually changes from woody savannah northward to short grass. The grassland–desert border is around 16.5°N. This vegetation distribution is used as the model's boundary condition over land. The soil texture ranges from silty loam (20% sand, 60% silt, and 20% clay) near the coast to loamy sand (80% sand, 10% silt, and 10% clay) in the north. South of the coast (set at 6°N), sea surface temperature (SST) is fixed at the zonal average (15°E–15°W) of its climatology (Reynolds and Smith 1995).

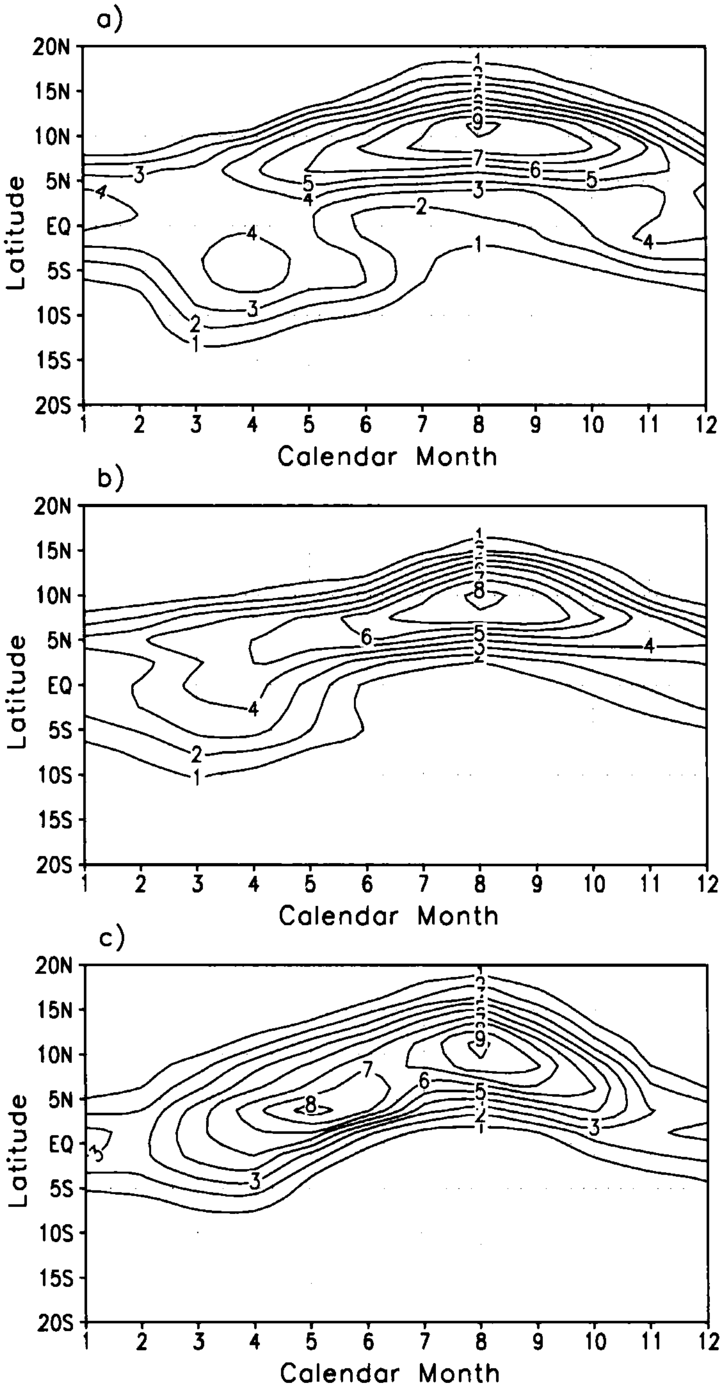

Figure 6. The seasonal cycle of rainfall (mm d^{-1}): (a) the model simulation; (b) climatology of the NCEP re-analysis data; and (c) climatology of the GPCP data.

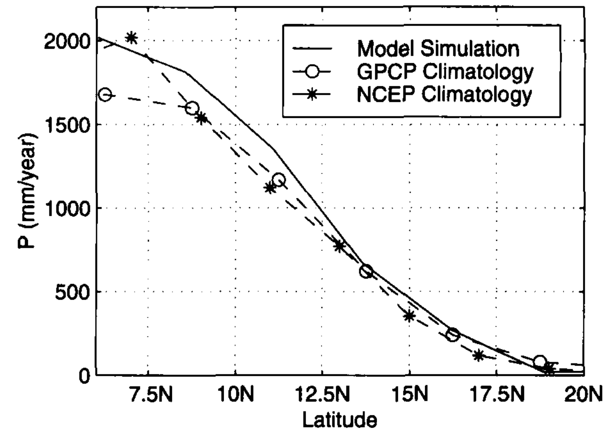

Figure 7. Comparison of annual rainfall between the model, the GPCP climatology, and the NCEP climatology.

For the simulation in this section as well as in section 4, we use a vertical resolution corresponding to about 40 mb, and a horizontal resolution corresponding to about $\sim 2.5°$ within the Tropics for both the biospheric model and the atmospheric model. The time-step is 20 minutes.

A zonally symmetric model cannot correctly simulate the interaction between mid-latitudes and the Tropics. To reduce the associated bias, surface conditions (including the albedo, temperature, sensible- and latent-heat fluxes) outside the Tropics are fixed at their climatology from the NCEP re-analysis data, averaged between 15°W and 15°E. Here the Tropics are defined as 27°N–27°S.

Three years of integration is needed before the atmospheric model reaches equilibrium, after which no trend is observed in the atmospheric simulation. Since we are using the SST climatology as the driving forcing, the simulated climate features negligible interannual variability after three years from the beginning of the simulation. In the following we present the results from the fourth year of the simulation.

Our zonally symmetric model successfully reproduces the zonal mean of precipitation and surface temperature in West Africa. The seasonal cycle of the simulated surface temperature is plotted in Fig. 5(a), which compares to the NCEP re-analysis data in Fig. 5(b) with good agreement. An identifiable difference is that the warm summer over the Sahara desert in the model lasts until October, which is about one month longer than that in the NCEP re-analysis data. Over West Africa, credible and inclusive rainfall measurement is limited. A significant discrepancy between different rainfall datasets is frequently observed, which causes difficulty in comparing rainfall simulation with observations. Here we compare the model rainfall seasonal cycle (Fig. 6(a)) with both NCEP re-analysis data (Fig. 6(b)) and the Global Precipitation Climatology Project (GPCP) data (Fig. 6(c)). The difference between the modelled rainfall seasonal cycle and either of the rainfall datasets is comparable to the difference between the GPCP data and the NCEP data. This is especially true over land, where the biosphere–atmosphere interactions of interest take place. The annual rainfall comparison over the land is presented in Fig. 7, which shows a fair agreement between the model simulation and observations.

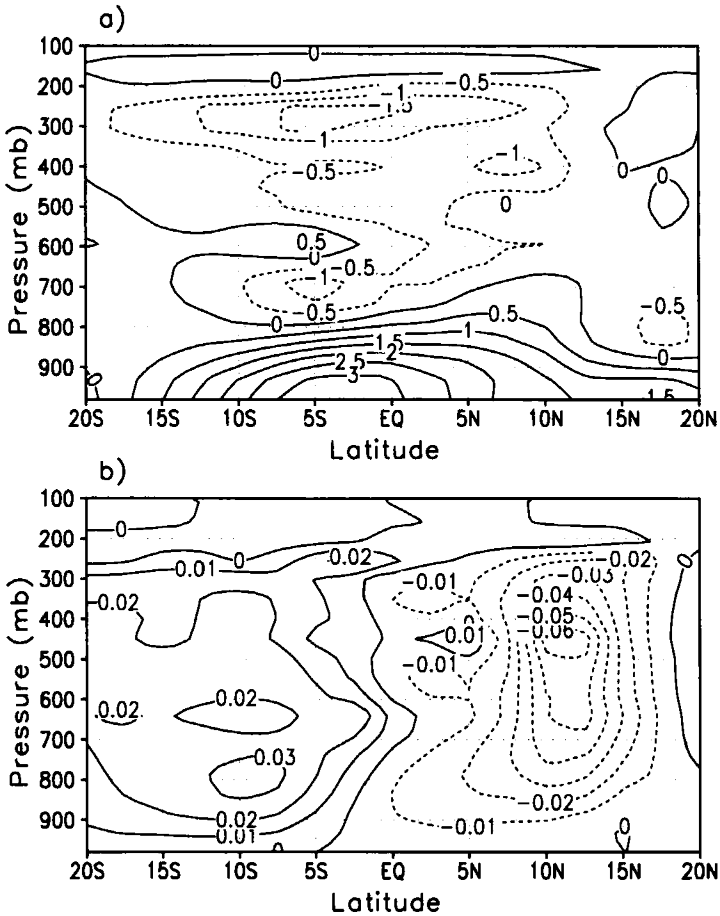

Figure 8. Comparison of the meridional circulation in August between the model and the NCEP re-analysis data. (a) Meridional wind from the model (m s^{-1}); (b) vertical velocity from the model (Pa s^{-1}); (c) meridional wind from the NCEP re-analysis data (m s^{-1}); and (d) vertical velocity from the NCEP re-analysis data (Pa s^{-1}). Negative contours are dashed.

The model also reproduces the meridional circulation with reasonable accuracy. As an example, Figs. 8(a) and (b) show the meridional cross-section of the simulated meridional wind and vertical velocity in August. The model captures the overall pattern of the monsoon circulation. During the rainy season, wind blows from the ocean to the land in the lower level, with the returning wind from the land to the ocean in the upper level. Correspondingly, the rising branch of the monsoon cell is mainly located over land, and the descending branch over the ocean. Compared to the NCEP re-analysis data (Figs. 8(c) and (d)), the model underestimates the magnitude of northward wind, but overestimates the vertical span of the northward wind. These two factors compensate for each other, which brings the total northward transport at low levels across the coast closer to the NCEP re-analysis data.

We compare the simulated net surface radiation with the climatology from the International Satellite Cloud Climatology Project (ISCCP) (Gupta *et al.* 1999), as shown in Figs. 9(a) and (b). The ISCCP data span from July 1983 to June 1991. Over the forest region in all seasons, and over the grassland during the rainy season, the

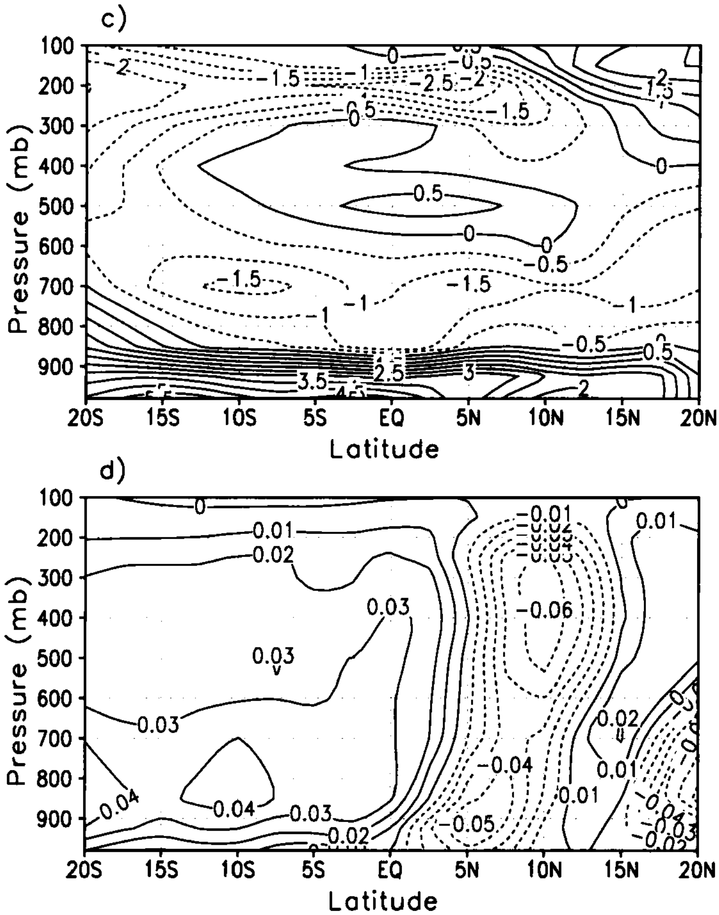

Figure 8. Continued.

difference between the simulation and the ISCCP climatology is within 20 W m^{-2}. Larger discrepancy exists over the grassland in the dry season and over the desert region all year long. While this may be a reflection of model deficit, it may also be due to the uncertainty of the ISCCP data. According to Bishop *et al.* (1997), inaccuracy in the ISCCP data is associated with the spatially and temporally varying aerosol distribution. It is worth noting that the largest discrepancy between the model and ISCCP data takes place where and when the ground is dry and unprotected, which tends to cause a high aerosol loading in the atmosphere.

Here we evaluate the representation of canopy hydrology using the fractional interception loss, as shown in Fig. 10. The fractional interception loss is defined as the fraction of the evapotranspiration that is contributed by the direct evaporation of the intercepted water on the canopy. According to Shuttleworth (1988a), the fractional interception loss is approximately 25% at a forest site in the Amazon. Our model estimation over the forest region is also around 25%. As expected, interception loss over savannah and grassland is much smaller, in the order of 10%.

In summary, the model reproduces the current atmospheric climate reasonably well.

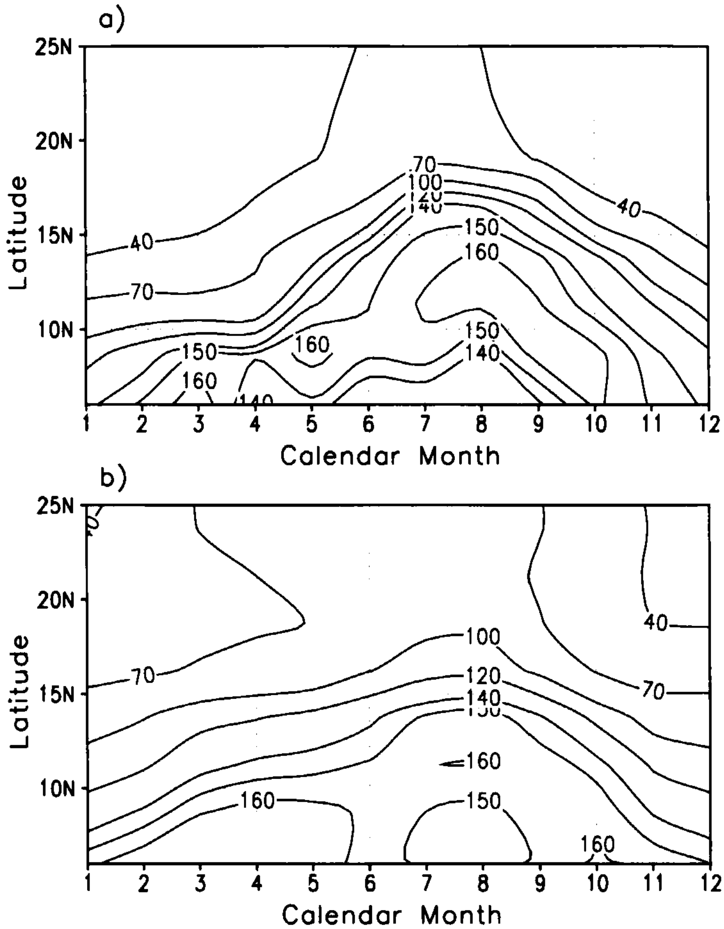

Figure 9. The seasonal cycle of net radiation at the surface (W m^{-2}): (a) from the model, and (b) from the ISCCP data.

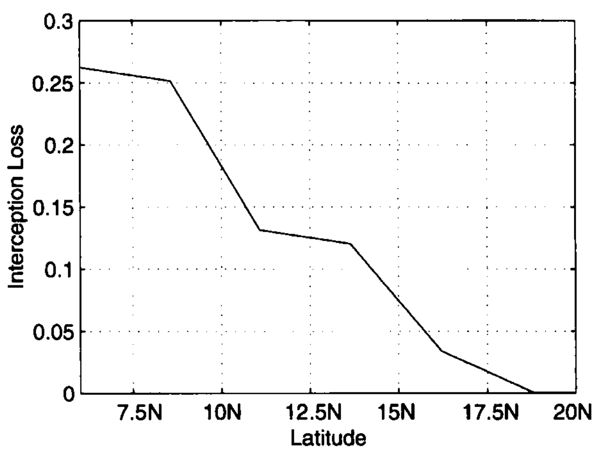

Figure 10. Interception loss as a fraction of the overall evapotranspiration.

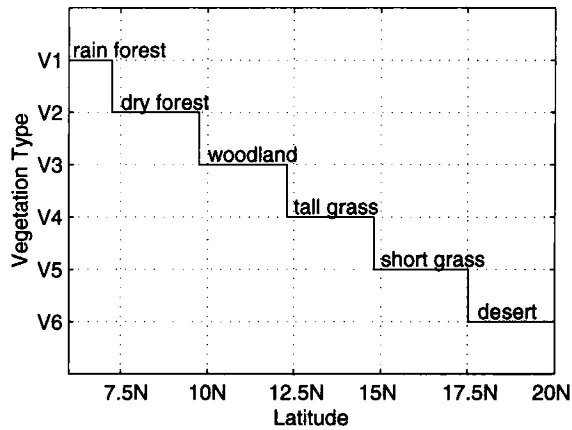

Figure 11. Distribution of vegetation type along the latitude at the attained biosphere–atmosphere equilibrium. The definition of vegetation type is the same as in Fig. 2.

4. Modelling the coupled biosphere–atmosphere system

After testing each of the two model components against observations, we run the synchronously coupled model including ecosystem dynamics to simulate the biosphere–atmosphere system of West Africa. The model starts with initial vegetation types close to today's condition, with vegetation dynamics simulated in the region between the coast (6°N) and 27°N. Similar to the simulation of section 3, surface properties and fluxes outside the Tropics are fixed at their climatological values from the NCEP re-analysis data, and SST is also fixed at the climatology (Reynolds and Smith 1995).

To allow the atmospheric model to spin up, vegetation in the first three years remains static. Ecosystem dynamics start to take place in the fourth year of simulation. The modelled system evolves into an equilibrium state within 25 years. An additional 15 years of simulation reveals no noticeable trend. Similar to today's environment in West Africa, this equilibrium state features forest in the south and grassland in the north, as shown in Fig. 11. However, in the region between the forest and the grassland, at a grid point near 11°N, the initialized savannah vegetation gives way to dense woodland. As demonstrated by the evolution of the growing-season LAI for the upper and lower canopy (Fig. 12), grasses at this savannah site become overwhelmingly dense immediately after the onset of vegetation dynamics, probably due to the lack of disturbances under a relatively wet climate; trees gradually develop and eventually shade grasses out. The annual rainfall at the model equilibrium is presented in Fig. 13. As a comparison, also presented in Fig. 13 is the annual rainfall simulated in section 3 with fixed current vegetation, which is comparable to the current climate (Fig. 7). In general, the climate of the equilibrium state is slightly wetter and greener than the current climate in West Africa.

Strictly speaking, the climate of the model equilibrium is not comparable with the observed current climate since the current biosphere–atmosphere system may not be at its natural equilibrium. First, it is uncertain whether the current system is at equilibrium at all; secondly, any equilibrium in the real world is expected to be different from the modelled natural equilibrium due to recurrent human activities.

Similar to the equilibrium biosphere in section 3, a very noticeable feature of the simulated biosphere–atmosphere equilibrium is the absence of savannah. As shown

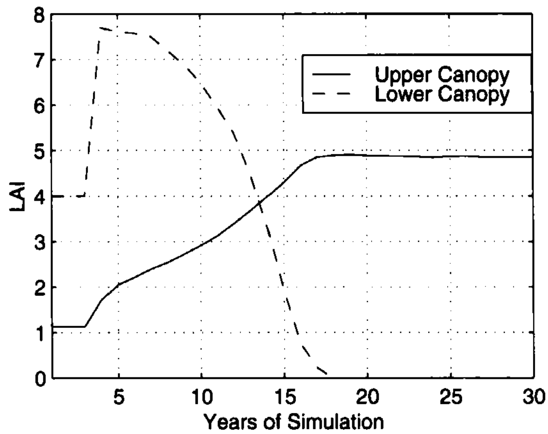

Figure 12. The evolutionary process of the growing-season leaf area index for the upper canopy and for the lower canopy at 11°N, where vegetation was initialized as savannah.

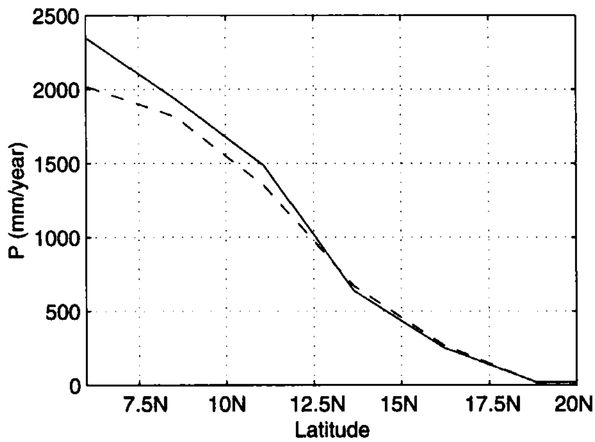

Figure 13. Distribution of annual rainfall along latitude, at the attained biosphere–atmosphere equilibrium (solid line). As a comparison, the dashed line plots the rainfall distribution modelled with fixed, 'close-to-current' vegetation.

in Fig. 12, trees eventually take over in the region that is initialized with savannah-type vegetation as observed. Although several studies (e.g. Eagleson and Segarra 1985; Rodriguez-Iturbe *et al.* 1999) argued that the savannah vegetation system is naturally stable, various ecological evidence suggests that the stability of savannah in some regions may depend on external disturbances. These disturbances can be of natural origin or anthropogenically induced. In many parts of West Africa, the savannah landscapes were originally created and are still maintained by recurrent burning for various human purposes (Bourliere and Hadley 1983). According to Bourliere and Hadley (1983), "*when plots of such man-maintained savannas are protected from bush fires for a number of years, they very quickly turn into deciduous woodland*". Grazing also plays an important role in maintaining the current savannah landscape in Africa (Sprugal 1991). For example, tree establishment over the current savannah region started around 1895 when the cattle disease 'rinderpest' was introduced into Africa (Sinclair 1979), and was suppressed again when vaccines were developed later on to protect

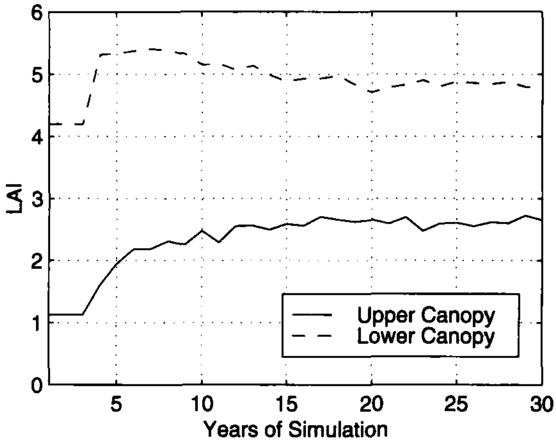

Figure 14. As Fig. 12, but with the impact of fire and grazing over the savannah and grassland region.

domestic livestock. Various human disturbance of such kinds left the current landscape as a mixture of grasses and trees. The transient nature of savannah-type vegetation in our model may have to do with the lack of representation of these various disturbances.

To qualitatively validate the above argument on the simulation of savannah-type vegetation, we perform one experiment with a certain degree of fire and grazing effect imposed over the savannah and grassland region. Fire is assumed to take place every year in the dry season and consumes a fraction f of the above-ground live biomass, where f varies from one year to the next and is a random number uniformly distributed between 0 and 10%. We assume that grazing consumes 50% of the grass NPP every year. Figure 14 shows the evolution of peak LAI for the upper and lower canopy at the grid point near 11°N, where initial vegetation is a mixture of trees and grasses. Under the impact of disturbances, the savannah-type vegetation survives into the model equilibrium. Comparison between Figs. 12 and 14 confirms that disturbances could indeed play an important role in the survival of savannah-type vegetation. This experiment is designed to investigate the qualitative impact of disturbances on the model's equilibrium state, therefore we made no effort to reproduce the historical occurrence of fire or grazing.

5. Conclusion

This paper presents our zonally symmetric model that describes the coupled biosphere–atmosphere system including ecosystem dynamics. The model has been applied to the region of West Africa, where climate conditions show a high degree of zonal symmetry. Experiments have been carried out to test both the biospheric model and the atmospheric model against observations and re-analysis data. Our results show that the model can reproduce the current biospheric climate and atmospheric climate in West Africa fairly well. However, since the real world is not zonally symmetric, we expect that there would be some differences between the model and observations, as shown in previous sections.

After separately validating the biospheric model and the atmospheric model, we simulate the natural climate system of West Africa using the synchronously coupled biosphere–atmosphere model. At equilibrium state, the climate of the natural biosphere–atmosphere system is close to, but slightly wetter and greener than, the current climate. Focusing on the natural interactions between the biosphere and the atmosphere, this study did not account for the historical occurrence of human perturbations. At present, it is impossible to identify whether the current observed climate system is at equilibrium; therefore, the comparison between the model equilibrium and the current climate may not be justifiable. Nevertheless, the model equilibrium that is 'close-to-current' provides an ideal control state for further studies.

ACKNOWLEDGEMENTS

We thank Dr Jonathan Foley and his group at the University of Wisconsin for sharing the dynamic biospheric model IBIS. We are grateful to Dr Xinyu Zheng and Julie Kiang for helpful discussions. Jeremy Pal deserves credit for his long-time help on computer-related issues. Comments from the anonymous reviewers significantly improved the quality of the paper. NCEP re-analysis data were provided by the NOAA-CIRES Climate Diagnostics Center, Boulder, Colorado. GPCP data were provided by the World Data Centre for Meteorology, NCDC, Asheville, NC. This research has been supported by the National Aeronautics and Space Administration (NASA) under agreement NAGW-5201, NAG5-7525, and NAG5-8617, and by the National Science Foundation (NSF) under agreement ATM 9807068. The views, opinions, and/or findings contained in this paper are those of the authors and should not be construed as an official NASA or NSF position, policy or decision, unless so designated by other documentation.

REFERENCES

Bishop, J. K. B., Rossow, W. B. and Dutton, E. G. 1997 Surface solar irradiance from the International Satellite Cloud Climatology Project 1983–1991. *J. Geophys. Res.*, **102,** 6883–6910

Bourliere, F. and Hadley, M. 1983 Present-day savannas: an overview. Pp. 1–17 in *Ecosystem of the world—tropical savannas*. Ed. F. Bourliere. Elsevier, New York

Brostrom, A., Coe, M., Harrison, S. P., Gallimore, R., Kutzbach, J. E., Foley, J. A., Prentice, I. C. and Behling, P. 1998 Land surface feedback and palaeomonsoons in northern Africa. *Geophys. Res. Lett.*, **25,** 3615–3618

Charney, J. G. 1975 Dynamics of deserts and drought in the Sahel. *Q. J. R. Meteorol. Soc.*, **101,** 193–202

Charney, J. G., Quirk, W. J., Chow, S. and Kornfield, J. 1977 A comparative study of the effects of albedo change on drought in semi-arid regions. *J. Atmos. Sci.*, **34,** 1366–1385

Chou, M.-D. 1984 Broadband water vapor transmission functions for atmospheric IR flux computations. *J. Atmos. Sci.*, **41,** 1775–1778

1986 Atmospheric solar heating rate in the water vapor bands. *J. Clim. Appl. Meteorol.*, **25,** 1532–1542

1990 Parameterizations for the absorption of solar radiation by O_2 and CO_2 with application to climate studies. *J. Clim.*, **3,** 209–217

1992 A solar-radiation model for use in climate studies. *J. Atmos. Sci.*, **49,** 762–772

Chou, M.-D. and Kouvaris, L. 1991 Calculations of transmission functions in the infrared CO_2 and O_3 bands. *J. Geophys. Res.*, **96,** 9003–9012

Chou, M.-D., Kratz, D. P. and Ridgway, W. 1991 Infrared radiation parameterizations in numerical climate models. *J. Clim.*, **4,** 424–437

Claussen, M. 1994 On coupling global biome models with climate models. *Clim. Res.*, **4,** 203–221

1997 Modeling bio-geophysical feedback in the African and Indian monsoon region. *Clim. Dyn.*, **13,** 247–257

Dickinson, R. E. and Henderson-Sellers, A. 1988 Modelling tropical deforestation: A study of GCM land-surface parametrizations. *Q. J. R. Meteorol. Soc.*, **114,** 439–462

Eagleson, P. S. and Segarra, R. I. 1985 Water-limited equilibrium of savanna vegetation systems. *Water Resour. Res.*, **21,** 1483–1493

Eltahir, E. A. B. and Bras, R. L. 1993 Estimation of the fractional coverage of rainfall in climate models. *J. Clim.*, **6,** 639–644

Emanuel, K. 1991 A scheme for representing cumulus convection in large-scale models. *J. Atmos. Sci.*, **48,** 2313–2335

Foley, J. A., Prentice, I. C., Ramankutty, N., Levis, S., Pollard, D., Sitch, S. and Haxeltine, A. 1996 An integrated biosphere model of land surface processes, terrestrial carbon balance, and vegetation dynamics. *Global Biogeochem. Cycles*, **10,** 603–628

Foley, J. A., Levis, S., Prentice, I. C., Pollard, D. and Thompson, S. L. 1998 Coupling dynamic models of climate and vegetation. *Global Change Biology*, **4,** 561–579

Gupta, S. K., Ritchey, N. A., Wilber, A. C., Whitlock, C. H., Gibson, G. G. and Stackhouse, P. W. 1999 A climatology of surface radiation budget derived from satellite data. *J. Clim.*, **12,** 2691–2710

Henderson-Sellers, A., Dickinson, R. E., Durbidge, T. B., Kennedy, P. J., McGuffie, K. and Pitman, A. J. 1993 Tropical deforestation: Modeling local- to regional-scale climate change. *J. Geophys. Res.*, **98,** 7289–7315

Holtslag, A. A. M. and Boville, B. A. 1993 Local versus non-local boundary-layer diffusion in a global climate model. *J. Clim.*, **6,** 1825–1842

Jackson, R. B., Canadell, J., Ehleringer, J. R., Mooney, H. A., Sala, O. E. and Schulze, E. D. 1996 A global analysis of root distributions for terrestrial biomes. *Oecologia*, **108,** 389–411

Johnson, K. D., Entekhabi, D. and Eagleson, P. S. 1991 The implementation and validation of improved land-surface hydrology in an atmospheric general circulation model. Technical Report No. 334, Ralph. M. Parsons Laboratory, MIT, Cambridge, Ma

Kalnay, E., Kanamitsu, M., Kistler, R., Collins, W., Deaven, D., Gandin, L., Iredell, M., Saha, S., White, G., Woollen, J., Zhu, Y., Chelliah, M., Ebisuzaki, W., Higgins, W., Janowiak, J., Mo, K. C., Ropelewski, C., Wang, J., Leetmaa, A., Reynolds, R., Jenne, R. and Joseph, D. 1996 The NCEP/NCAR 40-year re-analysis project. *Bull. Am. Meteorol. Soc.*, **77,** 437–471

Kutzbach, J., Bonan, G., Foley, J. and Harrison, S. P. 1996a Vegetation and soil feedbacks on response of the African monsoon to orbital forcing in the early to middle Holocene. *Nature*, **384,** 623–626

Kutzbach, J., Bartlein, P. J., Foley, J., Harrison, S. P., Hostetler, S. W., Liu, Z., Prentice, I. C. and Webb III, T. 1996b Potential role of vegetation feedback in the climate sensitivity of high-latitude regions: A case study at 6000 years BP. *Global Biogeochem. Cycles*, **10,** 727–736

Kvamsto, N. G. 1991 An investigation of diagnostic relations between stratiform fractional cloud cover and other meteorological parameters in numerical weather prediction models. *J. Appl. Meteorol.*, **30,** 200–216

Le Barbe, L. and Lebel, T. 1997 Rainfall climatology of the HAPEX-Sahel region during the years 1950–1990. *J. Hydrol.*, **188–189,** 43–73

Lebel, T., Taupin, J. D. and D'Amato, N. 1997 Rainfall monitoring during HAPEX-Sahel. 1. General rainfall conditions and climatology. *J. Hydrol.*, **188–189,** 74–96

Lofgren, B. M. 1995a Sensitivity of land–ocean circulations, precipitation, and soil moisture to perturbed land surface albedo. *J. Clim.*, **8,** 2521–2542

1995b Surface albedo–climate feedback simulated using two-way coupling. *J. Clim.*, **8,** 2543–2563

London, J. 1952 The distribution of radiational temperature change in the Northern Hemisphere during March. *J. Meteorol.*, **9,** 145–151

Mocko, D. M. and Cotton, W. R 1995 Evaluation of fractional cloudiness parameterizations for use in a mesoscale model. *J. Atmos. Sci.*, **52,** 2884–2901

Murphy, P. G. 1975 Net primary productivity in tropical terrestrial ecosystems. Pp. 217–231 in *Primary productivity of the biosphere*. Eds. H. Lieth and R. H. Whittaker. Springer-Verlag, New York

Nicholson, S. E. 1981 The historical climatology of Africa. Pp. 249–270 In *Climate and history*. Eds. T. M. L. Wigley *et al.* Cambridge University Press

Pitman, A. J., Henderson-Sellers, A. and Yang, Z.-L. 1990 Sensitivity of regional climates to localized precipitation in global models. *Nature*, **346**, 734–737

Plumb, R. A. and Hou, A. U. 1992 The response of a zonally symmetric atmosphere to subtropical thermal forcing: Threshold behaviour. *J. Atmos. Sci.*, **49**, 1790–1799

Reynolds, R. W. and Smith, T. M 1995 A high-resolution global sea surface temperature climatology. *J. Clim.*, **8**, 1571–1583

Rodriguez-Iturbe, I., D'Odorico, P., Porporato, A. and Ridolfi, L. 1999 Tree–grass coexistence in savannas: The role of spatial dynamics and climate fluctuations. *Geophys. Res. Lett.*, **26**, 247–250

Shukla, J., Nobre, C. and Sellers, P. J. 1990 Amazon deforestation and climate change. *Science*, **247**, 1322–1325

Shuttleworth, W. J. 1988a Evaporation from Amazonia rainforest. *Proc. R. Soc.*, **233**, 321–346

1988b Macrohydrology—the new challenge for process hydrology. *J. Hydrol.*, **100**, 31–56

Sinclair, A. R. E. 1979 Dynamics of the Serengeti ecosystem. Pp. 1–30 in *Serengeti—dynamics of an ecosystem*. Eds. A. R. E. Sinclair and M. Norton-Griffiths. University of Chicago Press, Chicago

Slingo, J. M. 1980 Cloud parametrization scheme derived from GATE data for use with a numerical model. *Q. J. R. Meteorol. Soc.*, **106**, 747–770

1987 The development and verification of a cloud prediction scheme for the ECMWF model. *Q. J. R. Meteorol. Soc.*, **113**, 899–927

Sprugel, D. G. 1991 Disturbance, equilibrium, and environmental variability—what is natural vegetation in a changing environment. *Biological Conservation*, **58**, 1–18

Sundqvist, H., Berge, E. and Kristjansson, J. E. 1989 Condensation and cloud parameterization studies with a mesoscale numerical weather prediction model. *Mon. Weather Rev.*, **117**, 1641–1657

Sud, Y. C. and Molod, A. 1988 A GCM simulation study of the influence of Saharan evapotranspiration and surface-albedo anomalies on July circulation and rainfall. *Mon. Weather Rev.*, **116**, 2388–2400

Texier, D., De Noblet, N., Harrison, S. P., Haxeltine, A., Jolly, D., Joussaume, S., Laarif, F., Prentice, I. C. and Tarasov, P. 1997 Quantifying the role of biosphere–atmosphere feedbacks in climate change: Coupled model simulations for 6000 years BP and comparison with palaeodata for northern Eurasia and northern Africa. *Clim. Dyn.*, **13**, 865–882

Thomas, G. and Henderson-Sellers, A. 1991 An evaluation of proposed representations of subgrid hydrologic processes in climate models. *J. Clim.*, **4**, 898–910

Wang, G. and Eltahir, E. A. B. 1998 Biosphere–atmosphere interactions: Representation of sub-grid spatial variability of rainfall interception. *Eos, Transactions, AGU*, **79**, 349

2000 Biosphere–atmosphere interactions over West Africa. II: Multiple climate equilibria. *Q. J. R. Meteorol. Soc.*, **126**, 1261–1280

Xue, Y. and Shukla, J. 1993 The influence of land surface properties on Sahel climate. Part I: Desertification. *J. Clim.*, **6**, 2232–2245

Zeng, N., Dickinson, R. E. and Zeng, X. 1996 Climate impact of Amazon deforestation—a mechanistic model study. *J. Clim.*, **9**, 859–883

Zhang, H. and Henderson-Sellers, A. 1996 Impacts of tropical deforestation. Part I: Process analysis of local climate change. *J. Clim.*, **9**, 1497–1517

Zheng, X. 1997 'Moist zonally symmetric models and their applications to West African monsoons'. PhD. Thesis, MIT

1998 The response of a moist zonally symmetric atmosphere to subtropical surface temperature perturbation. *Q. J. R. Meteorol. Soc.*, **124**, 1209–1226

Zheng, X. and Eltahir, E. A. B. 1997 The response to deforestation and desertification in a model of West African monsoons. *Geophys. Res. Lett.*, **24**, 155–158

1998 The role of vegetation in the dynamics of West African monsoons. *J. Clim.*, **11**, 2078–2096

Zheng, X., Eltahir, E. A. B. and Emanuel, K. A. 1999 A mechanism relating tropical Atlantic spring sea surface temperature and west African rainfall. *Q. J. R. Meteorol. Soc.*, **125**, 1129–1164

Zobler, L. 1986 A world soil file for global climate modeling. NASA, Washington, DC